Journal of Alloys and Compounds 652 (2015) 172–178

Contents lists available at ScienceDirect

Journal of Alloys and Compounds

journal homepage: http://www.elsevier.com/locate/jalcom

Electrochemical corrosion behavior of Pb–Ca–Sn–Sm grid alloy in H_2SO_4 solution

Sadegh Pour-Ali [a, *], Mohammad Mosallami Aghili [b], Ali Davoodi [a]

[a] Materials and Metallurgical Engineering Department, Faculty of Engineering, Ferdowsi University of Mashhad, 91775-1111, Mashhad, Iran
[b] Materials Science and Engineering Department, Science and Research Branch, Islamic Azad University, Tehran, Iran

ARTICLE INFO

Article history:
Received 13 May 2015
Received in revised form
26 August 2015
Accepted 27 August 2015
Available online 29 August 2015

Keywords:
Lead acid battery
Pb–Ca–Sn–Sm alloy
Samarium
Corrosion

ABSTRACT

The electrochemical corrosion behavior of Pb-0.23 wt.% Ca-0.93 wt.% Sn and Pb-0.23 wt.% Ca-0.92 wt.% Sn-0.18 wt.% Sm alloys in 4.8 M H_2SO_4 at 25 °C was studied using open circuit potential (OCP), cyclic polarization, electrochemical impedance spectroscopy (EIS), linear sweep voltammetry (LSV) and Mott–Schottky plot. The findings of this study show that the samarium added to Pb–Ca–Sn alloy increases the general corrosion resistance of this alloy and inhibits the growth of the anodic corrosion layer, it can promote the pitting corrosion tendency of Pb–Ca–Sn alloy. Mott–Schottky plot also reveals that the anodic films on Pb–Ca–Sn and Pb–Ca–Sn–Sm alloys at +1.5 V vs. SCE exhibit an n-type semi-conductive character. Sm increases the slope of Mott–Schottky plot, implying the reduction of the defect density within the anodic film, which is beneficial to increase the resistance of anodic film.

1. Introduction

Many researchers are studying on non-antimonial grid compositions in lead acid batteries to significantly reduce the cost of battery manufacturing process. The initial approach to solve this problem has been to use pure lead anodes or lead-calcium binary alloys. The use of pure lead gives rise to a strong, stable and dense oxide passive layer formation at the grid/active material interface which can reduce the anode dissolution and increase the active life of the battery [1,2]. However, this layer can be deleterious for reversibility and charging efficiency during charge–discharge cycles [3,4]. On the other hand, doping with Ca is seen to improve the reversibility and charging efficiency of the lead based anodes used in the lead acid batteries [5]. Several studies have looked at the nature of the passive film formed on the anode. The composition of the passive layer is a mixture of $PbSO_4/PbO_x$ ($1 < x < 2$). On the surface of the lead grid tetragonal-PbO is formed, which acts as an insulator toward current flow. On the surface of PbO, different forms of PbO_2 are formed. Above this, $PbSO_4$ or mixed sulfate deposits are formed. The layers of PbO_2 and $PbSO_4$ are semi-permeable in nature and allow selective transport of ionic species. The cumulative effect of these different oxide and sulfate layers is to prevent electronic and ionic flow thereby preventing reversible cycling of the anode [1,6]. Nowadays, the major grid material for lead acid batteries is the lead-calcium-tin (Pb–Ca–Sn) ternary alloy. This alloy is especially suitable for the maintenance-free lead acid battery, because it leads to lower water consumption from the electrolyte [7]. Based on the report by Slavkov et al. [1], doping with Sn and Ca leads to an increased corrosion rate as compared to pure lead anodes. In recent years, many efforts have been made to modify the composition of Pb–Ca–Sn alloys for improving the electrochemical behavior of this alloy in H_2SO_4 solution. Some studies also focused on the substitutes for the alloying elements in Pb–Ca–Sn.

According to the study on the Pb–Ca–Sn–Li anodes by Shervedani et al. [8], addition of lithium to Pb–Ca–Sn alloy increases corrosion resistance in equilibrium potential and inhibits the growth of the anodic corrosion layer. Similar conclusions were derived by Liu et al. [9] who suggested that the presence of cerium in Pb–Ca–Sn alloy inhibits the growth of the anodic corrosion layer and reduces the resistivity of the anodic Pb (II) film. Based on the report by Lin et al. [10], Ce can also rapidly decrease the oxygen and hydrogen evolution on Pb–Ca–Sn–Ce alloy and thereby promote the maintenance-free property of lead acid battery. In addition, Zhou et al. [11] found that samarium element as a substitute for the calcium in the Pb–Ca–Sn alloy can inhibit the growth of the anodic corrosion layer (PbO_2) and reduce the impedance of the anodic corrosion layer (PbO_2) formed on the lead alloy. Moreover, the rate

* Corresponding author. Tel.: +98 9368019898.
E-mail address: pourali2020@ut.ac.ir (S. Pour-Ali).

http://dx.doi.org/10.1016/j.jallcom.2015.08.223
0925-8388/

of the oxygen evolution at the Pb–Ca–Sm alloy is also lower than that at the Pb–Ca–Sn alloy. According to Prengaman [12], addition of Ag to a Pb–Ca–Sn alloy can enhance its corrosion resistance and creep resistance, thereby an improved battery durability is seen at high temperatures. As another alloying element for the lead grid alloy, tellurium has been reported by Guo et al. [7]. They reported that the addition of tellurium to lead can improve its durability, mechanical strength and anti-corrosive ability. As a result, new additives especially alkaline earth metals have been sought for introduction to the grid alloys to improve their performance. Metal elements such as samarium, strontium, cerium and lithium, whose electrode potentials are close or more negative than that of calcium, may be added into Pb–Ca–Sn alloys to improve the crystal grain structure and electrochemical behavior of these alloys. Among these alloying elements, there is no quantitative electrochemical information on the effect of samarium incorporation in Pb–Ca–Sn alloys. The aim of this study was to examine the anodic behavior of Pb–Ca–Sn–Sm alloy in sulfuric acid solution by electrochemical methods to clarify the possibility of its preparation as a positive grid material for lead acid batteries.

2. Experimental

2.1. Preparation of the testing alloys

The Pb–Ca–Sn–Sm alloy was prepared in three steps: (i) a sample of Pb–Ca alloy was prepared by mixing pure pellets of corresponding metals (typically 100 g of Pb with 5 g of Ca) and melted under argon atmosphere at 860 °C for 15 min, cooled down to 500 °C, kept under these conditions for 4 h to form homogeneous Pb–Ca alloy, then cooled to room temperature and used for next steps; (ii) a sample of Pb–Sm alloy was also prepared by mixing pure pellets of Pb with Sm powder (typically 100 g of Pb with 15 g of Sm) and melted under argon atmosphere at 1120 °C for 40 min, then cooled down to 700 °C, kept under these conditions for 4 h to form homogeneous Pb–Sm alloy, then cooled to room temperature and kept for further works; and the final step (iii) appropriate percent of the Pb–Ca and Pb–Sm alloys were mixed with Sn pellets, heated at 1100 °C for 20 min, cooled down to 500 °C, kept under these conditions for 4 h to form homogeneous Pb–Ca–Sn–Sm alloy, then cooled to room temperature and used for preparation of working electrodes. Casting process of grid alloys was accomplished in an electrical furnace equipped with a vibrating stage. The Pb–Ca–Sn and Pb–Ca–Sn–Sm alloys were prepared by mixing different amounts of Pb–Ca and Pb–Sm with Sn, and then analyzed in the same way by atomic absorption spectroscopy (AAS). Bulk homogeneity of the prepared alloys was determined by dissolution of local samples in acidic solution and analyzed again by AAS. The local samples were cut from bulk of the prepared alloys. Finally, two obtained alloys with chemical composition of Pb-0.23 wt.% Ca-0.93 wt.% Sn and Pb-0.23 wt.% Ca-0.92 wt.% Sn-0.18 wt.% Sm were selected and used as working electrodes for electrochemical studies.

2.2. Electrochemical experiments

A three-electrode setup was used to study the electrochemical behavior of Pb alloys. A sample was prepared from each alloy and connected to a copper wire to be used as working electrode for electrochemical measurements. The sides and other parts of the working electrode were covered with an epoxy resin to avoid any contact with electrolyte solution, except electrode surface exposing a 1 cm × 1 cm surface area of the alloy. A platinum counter-electrode and a saturated calomel reference electrode (SCE) were used to perform the electrochemical tests. All potentials reported in this paper were referred to SCE. The electrolyte was 4.8 M H_2SO_4 solution prepared from H_2SO_4 and double distilled water. Before each test, the working electrodes were mechanically polished by 1000# and 2000# SiC emery papers, then washed with double distilled water and a cathodic potential of −1.2 V was applied for 10 min in order to eliminate the oxides formed during pretreatment.

An EG & G potentiostat (Model 273A) and a Solartron frequency response analyzer (Model SI 1255) were employed to run the corrosion measurements: open circuit potential (OCP), cyclic voltammetry (CV), electrochemical impedance spectroscopy (EIS), linear sweep voltammetry (LSV) and Mott–Schottky analysis. For EIS test, the potential amplitude was set to 10 mV, peak-to-peak (AC signal), and the frequency range was set from 30000 to 0.1 Hz. In order to analyze the obtained impedance data, an appropriate model was used (ZView software). Mott–Schottky plot of the anodic film at +1.5 V was also carried out with a 10 mV s^{-1} scanning rate, the scanning potential range was from 0 V to +2.0 V, and the measured frequency was 1000 Hz. Cyclic potentiodynamic polarizations were also carried out in the aforementioned solution at 25 °C with the same positions where the EIS tests were carried out. These tests were performed by sweeping the potential at a scan rate of 1 mV s^{-1} from −0.2 to +2.4 V and then backed to form a hysteresis loop.

2.3. X-ray diffraction (XRD) and scanning electron microscopy (SEM) measurements

Phase composition and morphology of the surface of polarized electrodes were determined using X-ray diffractometry (PW 3040/60, X'Pert PRO, Netherlands) and SEM (MIRA3 TESCAN) techniques, respectively. XRD patterns were recorded using Cu Kα radiation (λ = 1.5418 A°), in the 2θ range of 15–45° with a scan rate of 0.03°/s. SEM was equipped with an Energy Dispersive Spectrometer (EDS) to provide the chemical analysis of the surface of grid alloys.

3. Results and discussion

3.1. Open circuit potential (OCP)

According to [5,7,13], PbO_2 is the major product of Pb anodic corrosion at high potentials. The amount of PbO_2 can be used to evaluate the extent of corrosion of the positive grid alloy. A potential of +1.6 V was chosen for the OCP test, because +1.6 V is the growth potential for PbO_2 on the positive grid alloys when the battery is undergoing a float charge. The open circuit potential behavior of Pb–Ca–Sn and Pb–Ca–Sn–Sm alloys is illustrated in Fig. 1. Working electrodes were charged at +1.6 V for 1 h and the decay curves of potential vs. time were recorded in an open circuit condition. At the beginning time, an induction period appears in the OCP curve. Based on the report by Shu et al. [7], the induction period is attributed to the transformation of PbO_2 into $PbSO_4$ during the self-discharging process. In other words, the induction period time is associated with the amount of PbO_2 formed on the lead alloy during the charging process. As can be seen from Fig. 1, the induction time of Pb–Ca–Sn–Sm electrode is shorter than that of the Pb–Ca–Sn electrode. Thus, it can be claimed that the Sm can inhibit the growth of PbO_2 on lead alloys during charging. It should be noted that the steady state potentials are −0.056 V and −0.084 V for Pb–Ca–Sn and Pb–Ca–Sn–Sm alloys, respectively, which are different by almost 0.028 V. Despite this small shift, the dynamic polarization behavior showed that the general corrosion behavior of Pb–Ca–Sn is improved by addition of Sm to this alloy.

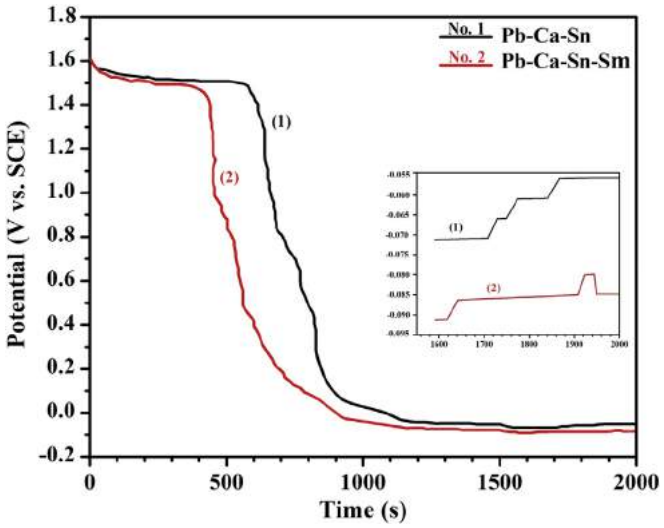

Fig. 1. The open circuit potential decay curves for the self-discharge of Pb–Ca–Sn and Pb–Ca–Sn–Sm electrodes after 1 h charging at 1.6 V in 4.8 mol L^{-1} H_2SO_4 solution.

3.2. XRD analysis

Fig. 2 shows the XRD patterns of Pb–Ca–Sn and Pb–Ca–Sn–Sm grid alloys before polarization and after different times of discharging. Unpolarized alloys show a characteristic peak of lead and there is no indication of the presence of other phases in their patterns. On the other hand, XRD patterns of polarized alloys are consisted of three phase peaks: (i) Pb: in each diagram, two large peaks attributed to this element are observed (similar to unpolarized samples), (ii) $PbSO_4$ and (iii) α-PbO_2. As can be clearly seen (Fig. 2), in the case of similar discharging times, relative diffraction intensity of $PbSO_4$ and α-PbO_2 peaks for Pb–Ca–Sn grid alloy is always higher than Pb–Ca–Sn–Sm one. It implies that the $PbSO_4$ and α-PbO_2 films on the surface of Pb–Ca–Sn alloy are thicker than Pb–Ca–Sn–Sm [14]. Thus, addition of 0.18 wt.% Sm can inhibit the growth of $PbSO_4$ and α-PbO_2 films during discharging and charging processes, respectively. This is in agreement with the results of OCP test.

3.3. Cyclic polarization

Fig. 3 presents the cyclic polarization curves of the Pb–Ca–Sn and Pb–Ca–Sn–Sm alloys for the potential range of −0.200 to +2.400 V. This test has been done to determine the pitting tendency and passivity current densities of the mentioned alloys. As can be clearly seen in Fig. 3, in the presence of Sm, passivity current density of Pb–Ca–Sn alloy severely decreases which can be an indication of low electronic exchange on the surface of this alloy. In addition, low passive current density hinders the passive film dissolution and enhances the corrosion resistance [15]. Despite of lower passive current density for Pb–Ca–Sn–Sm alloy, pitting corrosion behavior of this alloy is not ideal.

Pitting corrosion is a highly localized form of corrosion occurring on a metal surface. Pitting is commonly observed on surfaces with little or no general corrosion. Pitting typically occurs as a process of local anodic dissolution where metal loss is exacerbated by the presence of a small anode and a large cathode. During cyclic polarization test the potential is swept in the anodic direction until localized corrosion initiates as indicated by a large increase in the applied current. This occurs at approximately +2.0 V in Fig. 3. After this point, the direction of the scan is reversed, and the current

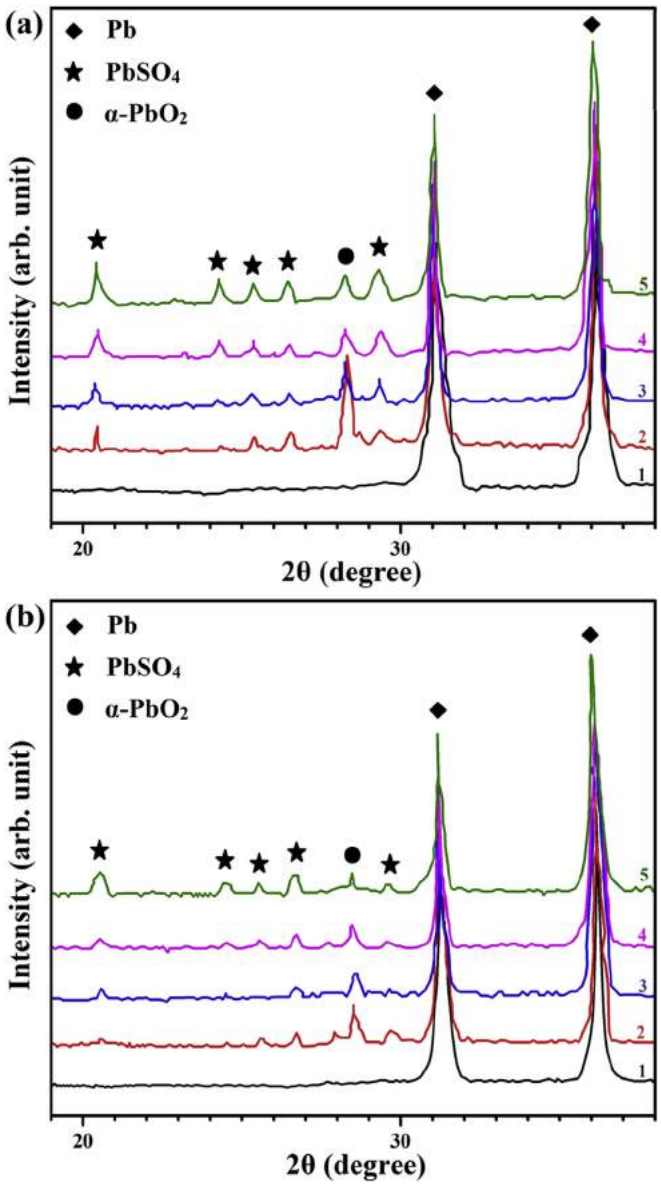

Fig. 2. XRD patterns of Pb-0.23 wt.% Ca-0.93 wt.% Sn (a) and Pb-0.23 wt.% Ca-0.92 wt.% Sn-0.18 wt.% Sm (b) alloys in unpolarized (1) and polarized conditions: anodized in 4.8 mol L^{-1} H_2SO_4 solution at 1.6 V after different discharging times: 300 s (2), 400 s (3), 500 s (4) and 600 s (5).

decreases until it changes polarity. E_{bd} (the breakdown potential) is the potential above which pits are initiated, while E_{rp} (the repassivation potential) is the potential below which pits repassivate. The E_{bd} is usually defined as the potential at which there is a large increase in the applied current, while the E_{rp} is the potential on the reverse scan at which the applied anodic current becomes zero (i.e. the current changes polarity). In Fig. 3, it can be also seen that the repassivation potentials are around +2.0 V and +1.5 V for the Pb–Ca–Sn and Pb–Ca–Sn–Sm alloys, respectively. These potentials correspond to the $PbO_2/PbSO_4$ couple. The higher E_{bd} for Pb–Ca–Sn indicates that this alloy is more resistant to the initiation of localized attack. Also, since E_{rp} is large and close to E_{bd}, this alloy can be easily repassivated. In the case of Pb–Ca–Sn–Sm alloy, large difference between E_{rp} and E_{bd} leads to enhanced propagation of sites which have initiated at E_{bd}. In fact, the larger hysteresis for Pb–Ca–Sn–Sm alloy, the more likely a localized corrosion site will

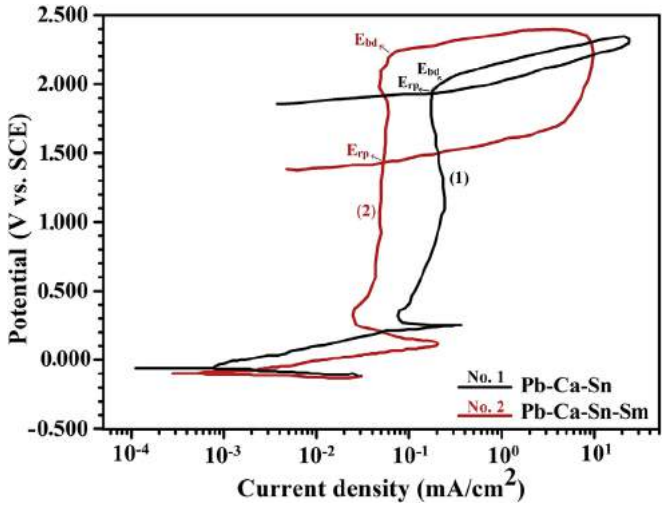

Fig. 3. Cyclic polarization plot of Pb–Ca–Sn and Pb–Ca–Sn–Sm alloys. E_{bd} and E_{rp} are the breakdown potential and the repassivation potential, respectively.

propagate once initiated. Fig. 4 shows the scanning electron microscopy (SEM) images and EDS results of Pb–Ca–Sn and Pb–Ca–Sn–Sm alloys which anodized at +1.6 V for 1 h (Fig. 4a and c) and after the completion of this test (Fig. 4b and d). Both alloys are consisted of a Pb-rich matrix with minor deviations in composition of alloying elements in both cases. In the Sm-containing alloy, distinct areas with higher concentration of samarium are seen after charging at +1.6 V for 1 h (Fig. 4c: areas 5, 6 and 7). As can be clearly seen in Fig. 4d, this alloy suffer from severe pitting corrosion after cyclic polarization test so that deep and large pits are formed on its surface. By comparing the distribution of Sm-rich compounds (Fig. 4c) with the locations of pits (Fig. 4d), it can be claimed that the Sm-rich compounds are responsible for the severe pitting corrosion. Based on these results, although Sm doping increases the stability of Pb–Ca–Sn alloy against general corrosion, aggressive pitting attack can threaten this alloy in the concentrated sulfuric acid electrolyte.

3.4. Impedance measurements

Electrochemical impedance spectroscopy (EIS) is a steady-state technique that can be used to study the oxide film on the surface and is frequently employed to investigate the characteristics of the oxide films on the surfaces of lead alloys. In the present investigation, this method was used to provide a consistent and alternative way to study the corrosion resistance of PbO_2 film on the mentioned lead alloys. Impedance measurements for Pb–Ca–Sn and Pb–Ca–Sn–Sm alloys were performed at a potential of +1.5 V with an AC voltage signal varying by ±10 mV, which ensures that the electrode system is under minimum perturbation. The EIS results in the form of Nyquist and Bode phase plots are presented in Fig. 5. It is obvious that the diameter of semicircle pertaining to Pb–Ca–Sn alloy impedance significantly increases by adding the Sm into this alloy. The addition of Sm does not change the typical shape of the Nyquist and particularly Bode phase plots which contain one time constant. For these corrosion reactions which are charge-transfer controlled, impedance behavior can be explained using a simple equivalent circuit containing a double layer capacitance (CPE_{dl}), charge transfer resistance (R_{ct}) and solution resistance (R_s). The resistor R_s is in series to the double layer capacitance and R_{ct} while the double layer capacitance is parallel to R_{ct} (see Fig. 6). The impedance parameters of the mentioned equivalent circuit that have been quantitatively extracted from the experimental data using EIS analyzer software are listed in Table 1. The values of CPE capacitance were calculated by using Eq. (1) [16]:

$$C_{dl} = P^{1/n} R_{ct}^{(1-n)/n} \quad (1)$$

In above expressions, P and n are the magnitude of CPE and deviation parameter (i.e. deviation of the semicircle from its ideal form), respectively. Table 1 shows that R_{ct} values increase with addition of Sm so that these values are 7065 and 11282 Ω cm^2 for Pb–Ca–Sn and Pb–Ca–Sn–Sm, respectively. In addition, the values of the double-layer capacitance (C_{dl}) decrease by adding Sm so that C_{dl} values reach 120 μF cm^{-2} considering 211 μF cm^{-2} for the Pb–Ca–Sn alloy. High amount of R_{ct} and lower value of C_{dl} are an indication of better corrosion performance of Pb–Ca–Sn–Sm alloy. Therefore, the EIS results also show that the corrosion resistance of Pb–Ca–Sn is substantially improved by the presence of Sm in this alloy.

3.5. Linear sweep voltammetry

The LSV is one of the most commonly used methods for evaluation of the electrochemical stability and corrosion resistance of the Pb grid alloys. In this test, the electrodes were anodized at +1.5 V in H_2SO_4 solution at 25 °C for 5, 25, 55, 85 and 145 min, and then the electrode potential was swept to −1.1 V with 1 mV s^{-1} scan rate to reduce the oxides formed. Fig. 7 shows a typical voltammogram of passive films formed on the Pb–Ca–Sn and Pb–Ca–Sn–Sm electrodes after 25 min anodization. The voltammograms for other anodization times are not shown since they are similar as that of the 25 min.

Peaks A and A′ are attributed to the reduction of Pb^{2+} to Pb, and peaks B and B′ to the reduction of $PbSO_4$ to Pb [8,17]. It can be seen that the current of peak A′ and B′ (for Pb–Ca–Sn–Sm electrode) is lower than that of A and B (for Pb–Ca–Sn electrode). This suggests that adding 0.18 wt.% Sm can inhibit the growth of both the $PbSO_4$ membrane and the anodic Pb (II) oxides film. This effect is proved with Fig. 8. As can be obviously seen, addition of Sm to the Pb–Ca–Sn alloy is beneficial to decrease the reduction charges for PbO + $PbO.PbSO_4$ (i.e., Pb^{2+}) and $PbSO_4$ to Pb. Variation of the anodic charges as functions of anodization time obtained for Pb–Ca–Sn and Pb–Ca–Sn–Sm show a linear behavior with slopes of 50C cm^{-2} s^{-1} and 20C cm^{-2} s^{-1} (for Pb^{2+}/Pb, i.e. Fig. 8a) and 10C cm^{-2} s^{-1} and 7C cm^{-2} s^{-1} (for $PbSO_4$/Pb, i.e. Fig. 8b), respectively. Therefore, addition of samarium into Pb–Ca–Sn alloy can clearly increase the corrosion resistance of this alloy.

3.6. Mott–Schottky analysis

The semi-conductive property of the passive film on metal or alloy is often studied by Mott–Schottky (M–S) analysis based on the measurement of the electrode capacitance as a function of the applied potential [18]. Assuming that the capacity of the Helmholtz layer is larger than that of the space charge region, the capacity of semiconducting passive layer follows the Mott–Schottky relationship:

$$\frac{1}{C_{CS}^2} = \frac{2}{\varepsilon\varepsilon_0 eN}\left(E - E_{fb} - \frac{kT}{e}\right) \quad (2)$$

Where C_{SC} is the charge space capacity, N the donor and/or acceptor densities, ε the relative electric permittivity, ε_0 the electric permittivity of vacuum, e the elementary charge, k the Boltzmann constant, T the absolute temperature, E_{fb} the flat band potential and E is the potential. The term KT/e can be neglected because it is only about 25 mV at room temperature. N can be determined from the

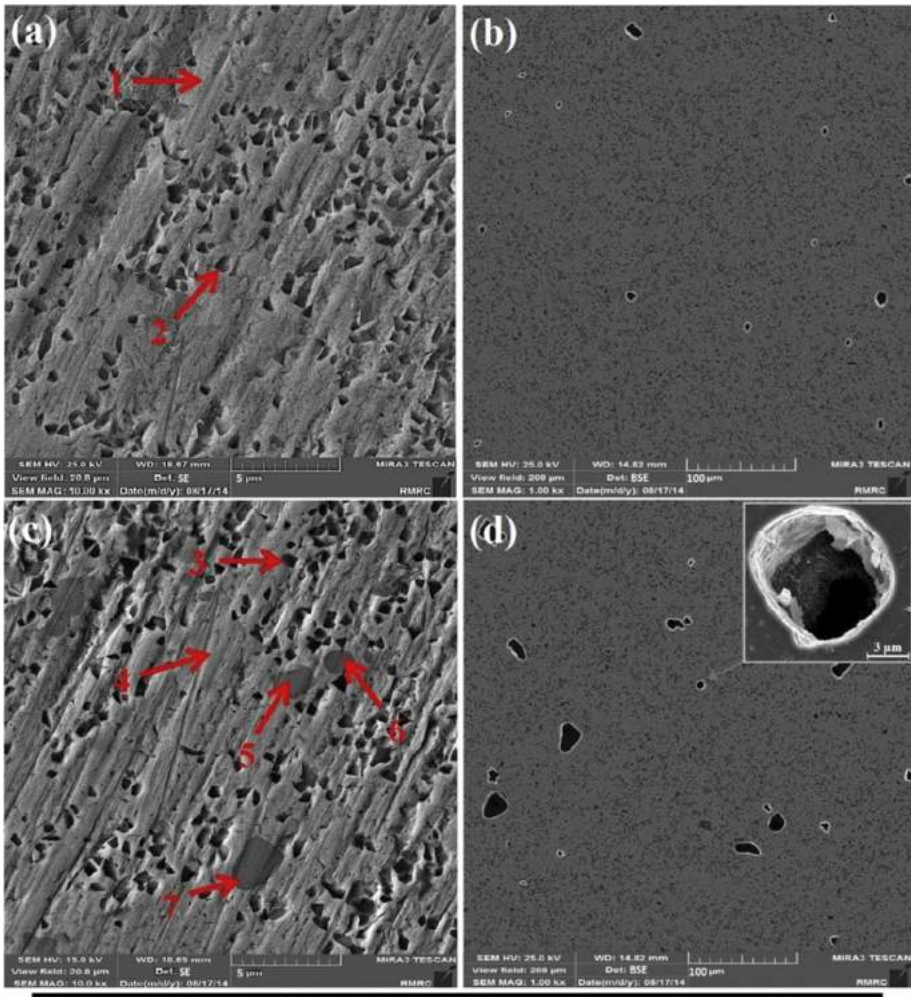

Position	1	2	3	4	5	6	7
Pb	Bal.	Bal.	Bal.	Bal.	Bal.	Bal.	Bal.
Ca	0.2	0.3	0.3	0.2	0.2	0.2	0.2
Sn	0.7	1.3	1.4	0.8	0.9	0.9	0.8
Sm	-	-	0.0	0.1	0.7	0.8	0.8

Fig. 4. SEM images of the surfaces of Pb–Ca–Sn and (a and b) Pb–Ca–Sn–Sm (c and d) grid alloys after anodic polarization for 1 h at 1.6 V (a and c) and after the completion of cyclic polarization test (b and d). Severity of pitting corrosion on the surface of Pb–Ca–Sn–Sm alloy is not negligible.

slope of the experimental C^{-2} versus E plot, and E_{fb} can be obtained from the extrapolation of the linear portion to $C^{-2} = 0$ [18,19]. Fig. 9 shows the Mott–Schottky plots of the anodic films on electrodes at +1.5 V recorded at 1 kHz with a rate of 10 mV s^{-1}, for 12 h in 4.8H_2SO_4 mol L^{-1} solution at 25 °C, in which the slopes of M–S plots exhibit a linear relationship with positive slope. As the slope is the indicator of the semiconductor type, it can be concluded that the anodic films formed on two electrodes exhibit n-type semiconductor character. In other words, since PbO_2 is an oxide conductor with interstitial cations (n-type semiconductor), it can be claimed that the majority of anodic film on the both Pb alloys comprise PbO_2. This result is consistent with previous study [13]. The slope of the M–S plot of Pb–Ca–Sn electrode is obviously lower than that of Pb–Ca–Sn–Sm electrode, and that demonstrates the donor density of the anodic film on Pb–Ca–Sn electrode is higher than that on Pb–Ca–Sn–Sm electrode. The calculated values of donor densities for the anodic films (Eq. (2)) formed on Pb–Ca–Sn and Pb–Ca–Sn–Sm electrodes are 6.08 × 10^{17} and 4.94 × 10^{16} cm^3, respectively. This significant difference implies that the defect density within the anodic film decreases meaningfully with the addition of Sm based on Eq. (2). Since defects existed in the anodic film can act as charge carriers, less defect densities is an indication of improved resistivity of the anodic film. Therefore, the result in this section confirms other electrochemical test outcomes.

4. Conclusion

1. The addition of Sm element into Pb–Ca–Sn ternary alloy can significantly affect its electrochemical corrosion behavior in

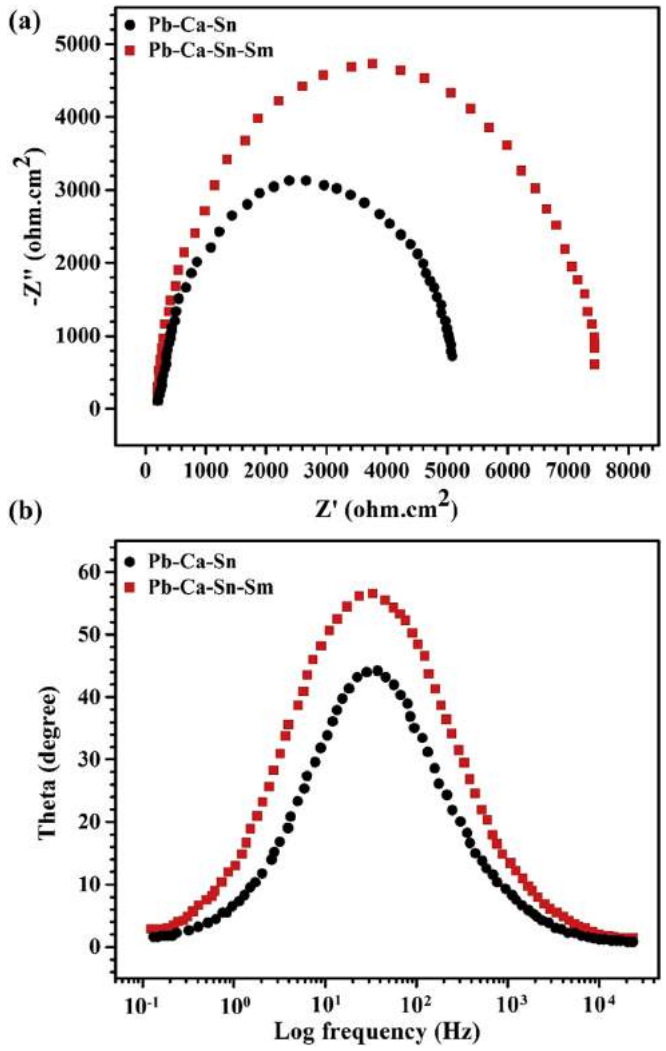

Fig. 5. (a) Nyquist and (b) Bode phase plots obtained for Pb–Ca–Sn and Pb–Ca–Sn–Sm alloys in 4.8 mol L^{-1} H_2SO_4 solution.

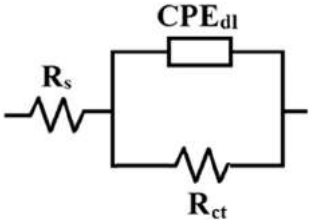

Fig. 6. The electrical equivalent circuit used to fit the impedance data of Pb–Ca–Sn and Pb–Ca–Sn–Sm alloys from Fig. 5.

Table 1
Fitted values calculated from the impedance data of Pb–Ca–Sn and Pb–Ca–Sn–Sm alloys using an equivalent circuit (Fig. 6).

Sample	R_s (Ω cm^2)	R_{ct} (Ω cm^2)	C_{dl} (μF cm^{-2})	CPE	
				P (μF cm^{-2})	n
Pb–Ca–Sn	4.1	7065	211	19	0.83
Pb–Ca–Sn–Sm	6.3	11282	120	17	0.86

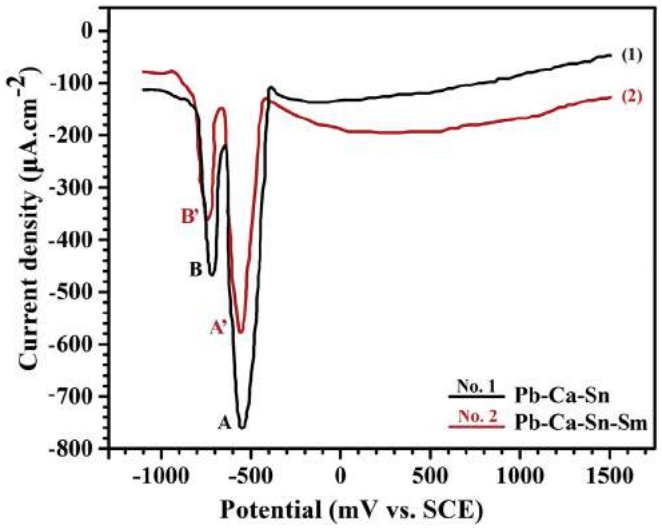

Fig. 7. Linear sweep voltammograms obtained for anodic films formed on (1) Pb–Ca–Sn and (2) Pb–Ca–Sn–Sm electrodes after 25 min anodization at +1.5 V in 4.8 M H_2SO_4 at 25 °C and then sweeping the potential to −1.1 V.

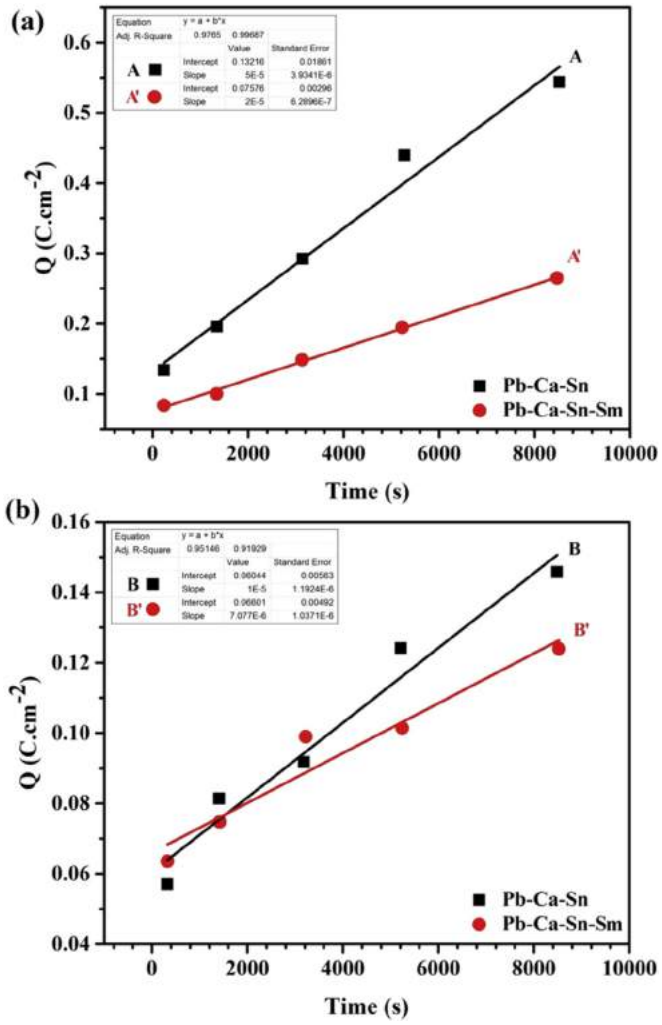

Fig. 8. Variation of reduction charges vs. anodization times for four peaks are shown in Fig. 7.

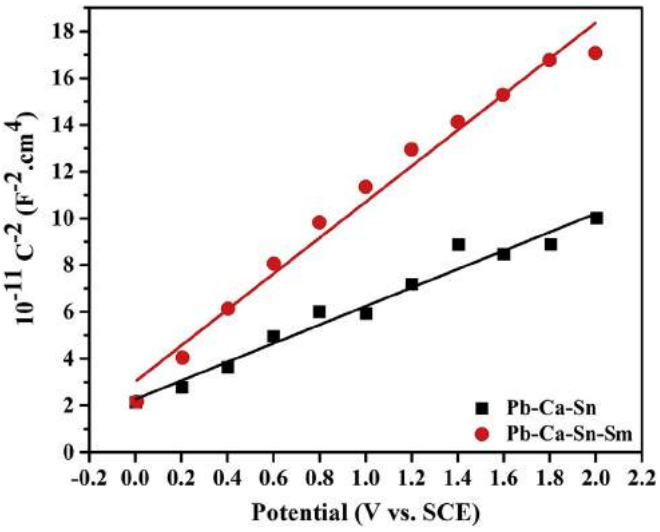

Fig. 9. Mott–Schottky plots of anodic films formed on two alloy electrodes.

4.8 mol L^{-1} H_2SO_4 solution at 25 °C. Sm decreases the passivity current density and inhibit the growth of anodic film at +1.5 V.

2. Cyclic potentiodynamic measurements revealed remarkable pitting corrosion for the Pb–Ca–Sn–Sm alloy. Based on SEM/EDS results, formation of Sm-rich compounds can be considered as a reason for such behavior.
3. Variation of the anodic charges as a function of anodization time showed that Sm can hinder the growth of both $PbSO_4$ and oxide films, and confirmed the increased corrosion resistance of Pb–Ca–Sn–Sm alloy. These results were in full agreement with EIS measurements.
4. The anodic films of Pb–Ca–Sn and Pb–Ca–Sn–Sm alloys appeared n-type semi-conductive character, the defect density within the anodic film on the Pb–Ca–Sn alloy decreased in the presence of Sm.

Acknowledgment

The authors gratefully acknowledge the support and generosity of the Kavosh Sanat Toos Co., specially Mr. Seyyed Alireza Naseri Hoseini and Mr. Hashem Teimoori, for consultation and assistance in casting process of lead alloys. Mr. Mohsen Noroozi, Mr. Mahdi kamali and Mr. Ramin Dallal-Moghaddam are also acknowledged for invaluable discussions.

References

[1] D. Slavkov, B.S. Haran, B.N. Popov, F. Fleming, Effect of Sn and Ca doping on the corrosion of Pb anodes in lead acid batteries, J. Power Sources 112 (2002) 199–208.
[2] Z.I. Takehara, Dissolution and precipitation reactions of lead sulfate in positive and negative electrodes in lead acid battery, J. Power Sources 85 (2000) 29–37.
[3] N. Sugumaran, P. Everill, S.W. Swogger, D.P. Dubey, Lead acid battery performance and cycle life increased through addition of discrete carbon nanotubes to both electrodes, J. Power Sources 279 (2015) 281–293.
[4] T. Tsujikawa, T. Matsushima, K. Yabuta, T. Matsushita, Estimation of the lifetimes of valve-regulated lead-acid batteries, J. Power Sources 187 (2009) 613–619.
[5] M.M. Burashnikova, I.V. Zotova, I.A. Kazarinov, Pb-Ca-Sn-Ba grid alloys for valve-regulated lead acid batteries, Engineering 5 (2013) 9–15.
[6] M. Clancy, C.J. Bettles, A. Stuart, N. Birbilis, The influence of alloying elements on the electrochemistry of lead anodes for electrowinning of metals: a review, Hydrometallurgy 131–132 (2013) 144–157.
[7] W.X. Guo, D. Shu, H.Y. Chen, A.J. Li, H. Wang, G.M. Xiao, C.L. Dou, S.G. Peng, W.W. Wei, W. Zhang, H.W. Zhou, S. Chen, Study on the structure and property of lead tellurium alloy as the positive grid of lead-acid batteries, J. Alloys Compd. 475 (2009) 102–109.
[8] R.K. Shervedani, A.Z. Isfahani, R. Khodavisy, A. Hatefi-Mehrjardi, Electrochemical investigation of the anodic corrosion of Pb-Ca-Sn-Li grid alloy in H_2SO_4 solution, J. Power Sources 164 (2007) 890–895.
[9] H.T. Liu, J. Yang, H.H. Liang, J.H. Zhuang, W.F. Zhou, Effect of cerium on the anodic corrosion of Pb-Ca-Sn alloy in sulfuric acid solution, J. Power Sources 93 (2001) 230–233.
[10] G. Lin, G. Zhou, D. Li, M. Zheng, Effect of cerium on gas evolution behavior of Pb-Ca-Sn alloy, J. Rare Earths 24 (2006) 232–237.
[11] Y.B. Zhou, C.X. Yang, W.F. Zhou, H.T. Liu, Comparison of Pb-Sm-Sn and Pb-Ca-Sn alloys for the positive grids in a lead acid battery, J. Alloys Compd. 365 (2004) 108–111.
[12] R.D. Prengaman, Challenges from corrosion-resistant grid alloys in lead acid battery manufacturing, J. Power Sources 95 (2001) 224–233.
[13] L.C. Peixoto, W.R. Osório, A. Garcia, Microstructure and electrochemical corrosion behavior of a Pb-1wt% Sn alloy for lead-acid battery components, J. Power Sources 192 (2009) 724–729.
[14] N. Stein, G. Bourguignon, L. Raboin, L. Broch, L. Johann, E. Rocca, In situ ellipsometric and electrochemical monitoring of the oxidation of a Pb-Ca-Sn alloy used in the lead acid batteries, Thin Solid Films 455 (2004) 735–741.
[15] C.A. Della Rovere, J.H. Alano, R. Silva, P.A.P. Nascente, J. Otubo, S.E. Kuri, Characterization of passive films on shape memory stainless steels, Corros. Sci. 57 (2012) 154–161.
[16] B. Hirschorn, M.E. Orazem, B. Tribollet, V. Vivier, I. Frateur, M. Musiani, Determination of effective capacitance and film thickness from constant-phase-element parameters, Electrochim. Acta 55 (2010) 6218–6227.
[17] H. Chen, S. Li, A. Li, D. Shu, W. Li, C. Dou, Q. Wang, G. Xiao, S. Peng, S. Chen, Lead-samarium alloys for positive grids of valve-regulated lead-acid batteries, J. Power Sources 168 (2007) 79–89.
[18] D. Li, J. Wang, D. Chen, Influence of ytterbium on the electrochemical property of PbCaSn alloy in sulfuric acid solution, J. Power Sources 210 (2012) 163–171.
[19] K. Darowicki, S. Krakowiak, P. Ślepski, Selection of measurement frequency in Mott-Schottky analysis of passive layer on nickel, Electrochim. Acta 51 (2006) 2204–2208.